Original paper

U–Th-rich zircon, thorite and allanite-(Ce) as main carriers of radioactivity in the highly radioactive ultrapotassic melasyenite porphyry from the Šumava Mts., Moldanubian Zone, Czech Republic

Vladimír ŽÁČEK[1*], Radek ŠKODA[2], Petr SULOVSKÝ[3]

[1] *Czech Geological Survey, P. O. BOX 85, Klárov 3, 118 21 Prague 1, Czech Republic; vladimir.zacek@geology.cz*
[2] *Department of Geological Science, Faculty of Sciences, Masaryk University, Kotlářská 2, 611 37 Brno, Czech Republic*
[3] *Department of Geology, Faculty of Science, Palacký University, tř. Svobody 26, 779 00 Olomouc, Czech Republic*
[*] *Corresponding author*

A melasyenite porphyry from the vicinity of Kašperské Hory (the Šumava Mts., Moldanubian Zone) shows a high natural radioactivity (K = 4.4–6.1 wt. %, eU = 15–24 ppm, eTh = 38–49 ppm). The most important carriers of U and Th are zircon, thorite, allanite-(Ce) and scarce monazite. Most of the zircon and thorite grains are altered by post-magmatic processes due to which especially zircon shows a large degree of chemical variability. Primary magmatic zircon is nearly stoichiometric, poor in ThO_2 (up to 0.13 wt. %) and UO_2 (up to 0.42 wt. %). It often encloses strongly altered U- and Th-rich cores. These cores show a conspicuous zoning in the BSE. The bright zones are enriched in UO_2 (0.66–1.36 wt. %) and ThO_2 (0.21–0.94 wt. %) whereas the darker zones are highly enriched in CaO (up to 5.19 wt. %), with UO_2 contents ranging between 0.95 and 2.15 wt. % and the ThO_2 between 0.99 and 1.67 wt. %. The first percolation point of zircon was estimated at 0.4 $D_{[dpa]}$. Thorite is also strongly altered, being depleted in Y,REE and Si in its more hydrated parts. A further consequence are strongly varying UO_2 contents (1.79–27.60 wt. %) and locally enriched ZrO_2 (up to 10.92 wt. %), P_2O_5 (0.22–6.39 wt. %) and Y,REE (0.73–12.81 wt. % of REE_2O_3 and Y_2O_3 combined). Elevated amounts of Fe, Ca, Pb, As, Al, S, and Ti were detected in the most hydrated parts. Allanite-(Ce) is weakly zoned with 0.20–1.22 wt. % ThO_2 and up to 0.11 wt. % UO_2. Scarce monazite-(Ce) has the ThO_2 contents (13.57–15.85 wt. %) strongly prevailing over UO_2 (1.51–1.91 wt. %).

Keywords: melasyenite porphyry, radioactivity, zircon, thorite, allanite-(Ce), Moldanubicum, Bohemian Massif
Received: 16 August 2007; accepted 9 December 2009; handling editor: M. Štemprok

The online version of this article (doi: 10.3190/jgeosci.053) contains supplementary electronic material.

1. Introduction

Gneisses and migmatites in the Moldanubian Zone of the Šumava Mts. (southern part of the Bohemian Massif, Czech Republic, Fig. 1a) are frequently intruded by dykes post-dating the Variscan regional metamorphism (leucogranites, lamprophyric rocks, and various porphyries). Numerous occurrences of these dykes were recorded during the 1 : 25 000 scale mapping by the geologists of the Czech Geological Survey. The distribution of the dykes is highly irregular as shown in the published or manuscript maps (for detailed geology see Babůrek et al. 2000; Žáček et al. 2005; Žáček and Sulovský 2005).

Melasyenite porphyry shows the highest natural radioactivity of all the rocks in the region. The dykes of melasyenite porphyry form two swarms: northern one, in the vicinity of Kašperské Hory and Nezdice, and southern one, following approximately the line between Svojše and Stachy (Fig. 1b). Melasyenite porphyry dykes are absent, or very scarce, south of this area but they appear to continue eastwards, out of the area shown in Fig. 1. As noted e.g. by Holub (1997), the melasyenite porphyry dykes occupy a large zone of an approximately triangular shape and a length of about 115 km (NE–SW) at a width of *c.* 50 km. The area studied lies at the southern and western limit of this large zone.

The dyke swarms strike generally E–W of ENE–WSW, and cut Variscan metamorphic rocks, mainly migmatite, gneiss and the pre-Variscan orthogneiss bodies (Fig. 1b). The width of the dykes varies from 1–2 m to 10–20 m; the length some of them exceeds 1–2 km. This paper contributes to the mineralogy of a highly radioactive melasyenite porphyry and it is particularly focused on its accessory minerals as the main carriers of radioactivity.

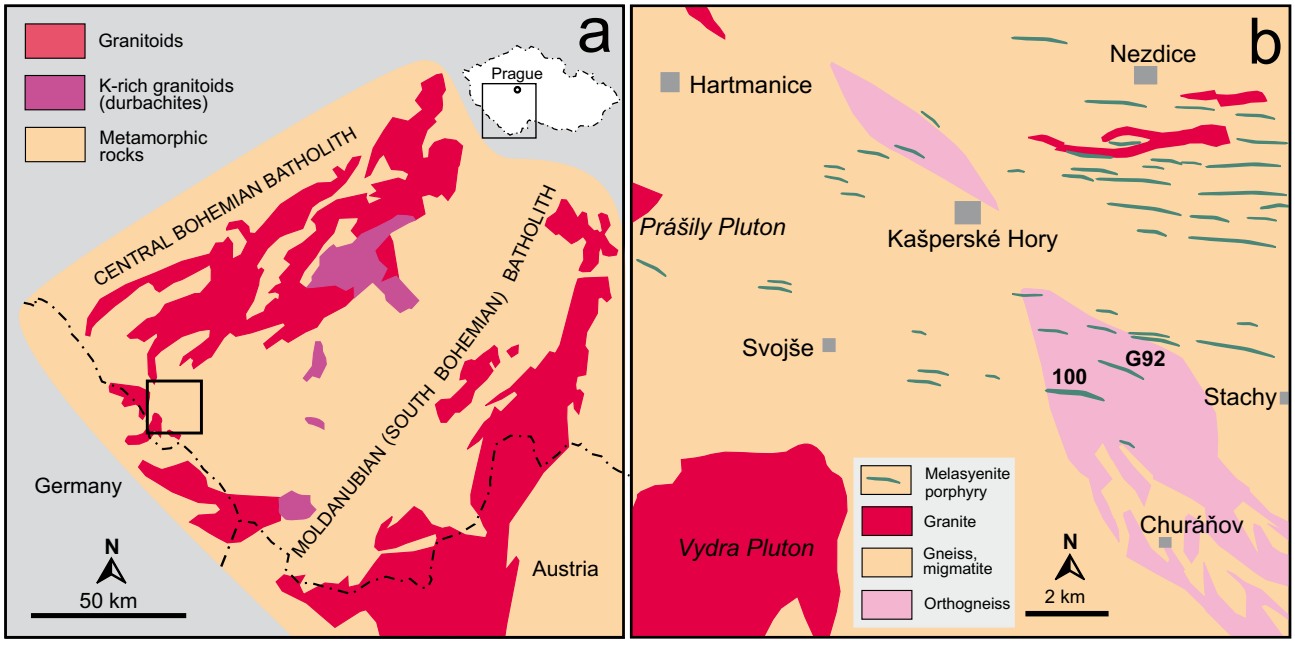

Fig. 1a – Map of the southern part of the Bohemian Massif showing the main Variscan batholiths. Frame indicates the area enlarged in Fig. 1b. **b –** Geological sketch of the area studied (following 1 : 25 000 maps of Babůrek et al. 2000 and Žáček et al. 2005).

2. Geological setting

2.1. Mineralogy, geochemistry and physical properties of the melasyenite

The melasyenite porphyry shows only limited variations in the petrography of individual dykes. It displays a "durbachitic" appearance with conspicuous phenocrysts (up to *c.* 1 cm) of K-feldspar and dark mica and green amphibole, visible with naked eye, set in a fine- to medium-grained matrix. The minerals are mostly randomly oriented or show slight fluidal alignment. The rock is composed of potassium feldspar (~ 40 vol. %, with up to 1.7 wt. % BaO and 0.42 wt. % SrO in phenocrysts; in contrast, fine potassium feldspar in the matrix is poor in Ba and Sr), ~ 20 vol. % of oligoclase ($An_{12–13}$), minor quartz, ~ 5 vol. %; ~ 10–15 vol. % of brown Ti-rich phlogopite (X_{Mg} = 0.65), and about the same amount of actinolite (X_{Mg} = 0.74, Si = 7.7–7.9 apfu) (Fig. 2). The samples of two dykes, which were studied in detail by electron microprobe, are situated south of Kašperské Hory (Fig. 1b) – the first one 1 km NW of Valy Hill (1010 m), 1.5 km WNW of Popelná (***sample 100***, 49°06'13.47"N, 13°23'9.99"E); the other one 400 m N of the settlement Frejd, 2 km SW of Nicov (***sample G92***, 49°06'38.10N, 13°36'24.25"E). The third chemical analysis (Table 1) is from a melasyenite porphyry outcrop situated at the railway between Bohumilice and Čkyně ***(sample SZ 110***, 49°06'27.03"N, 13°48'52.57"E), close to the eastern border of the area shown in Fig. 1b.

The melasyenite porphyry corresponds in terms of its texture, structure and chemical composition to (quartz) melasyenites – durbachites, typical of many parts of the Variscan orogenic belt where they are associated with exhumed lower-crustal metamorphic rocks of the former orogenic root (see e.g. Holub 1997; Janoušek and Holub 2007). The studied rock is intermediate to acid (63–64 wt. % SiO_2), metaluminous (A/CNK ~ 0.80) and calc-alkaline (straddling the boundary of the shoshonitic domain). Moreover, it is characterized by a high *mg* number as well as elevated Ti, P, Cr, Ni, Ba, Sr, Rb, Nb, U, Th and light REE (LREE) contents (Tab. 1); the REE pattern contains a sizeable negative Eu anomaly (Eu/Eu* ~ 0.5). Holub (2009) mentioned that average content (of 38 analyses) of SiO_2 is 63 wt. % and K_2O 6.4 wt. %. The concentrations of Th typically vary between 27 and 50 ppm and U between 15 and 23 ppm.

The melasyenite porphyry shows a weak magnetic susceptibility (0.13–0.31×10^{-3} SI) and typically a high natural radioactivity, the highest of the rocks in the area studied (Fig. 3). The concentrations of radioactive elements (measured by field gamma spectrometry) range between 4.4 and 6.1 wt. % for K, 15–24 ppm for eU and 38–49 ppm for eTh (15 measurements at 8 different dykes in a wider area).

2.2. Accessory minerals

The following accessory minerals were found in the two samples studied: titanite (~3 %), apatite (~1 %) >

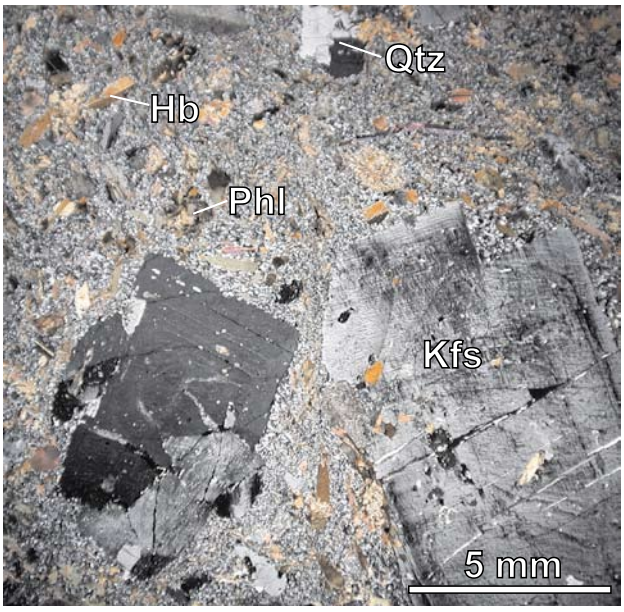

Fig. 2 Melasyenite porphyry, sample 100. Large crystals of potassium feldspar (Kfs) in much finer matrix, with abundant phlogopite (Phl), green actinolite (Hb) and quartz (Qtz). Image 15×15 mm, crossed polarizers. Photo V. Žáček.

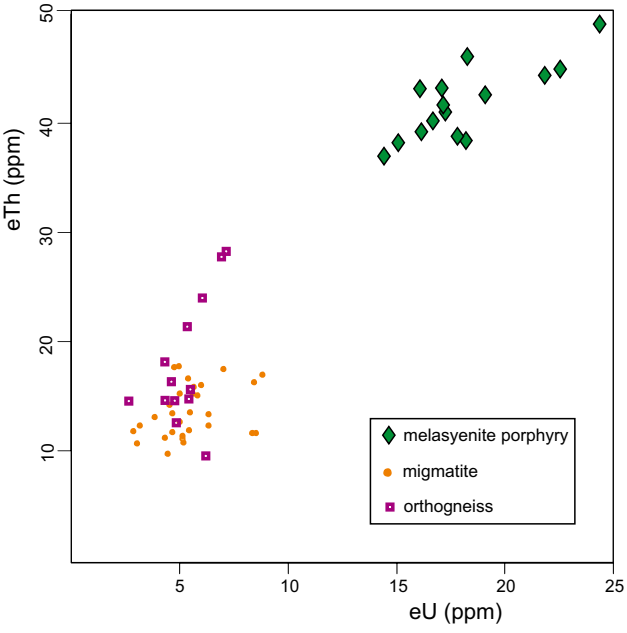

Fig. 3 eU versus eTh values for melasyenite porphyry, compared to the surrounding migmatite and orthogneiss (GRM-260 gamma spectrometry measurements).

zircon ~ allanite > thorite > monazite-(Ce). ***Titanite*** is abundant as brown subhedral aggregates up to 1–2 mm across. ***Fluorapatite*** forms prismatic euhedral to subhedral crystals from several µm to 1 mm across. Anhedral to subhedral grains or aggregates of ***allanite,*** reaching 50–500 µm in size, in the BSE (back-scattered electrons)

Table 1. Chemical composition of the melasyenite porphyry

	Kvilda 100	Čkyně SZ110	Kašp. H. KH11*
SiO_2	63.33	64.39	63.64
TiO_2	0.84	0.72	0.75
Al_2O_3	13.46	13.10	13.38
Fe_2O_3	1.40	1.15	0.95
FeO	2.84	2.75	2.91
MgO	4.28	4.08	4.46
MnO	0.08	0.07	0.07
CaO	2.82	2.12	2.46
BaO	0.13	0.15	0.26
Li_2O	0.01	0.01	0.01
Na_2O	2.43	2.47	2.34
K_2O	6.23	6.21	6.31
P_2O_5	0.55	0.61	0.62
F	0.15	0.15	0.03
H_2O^+	1.24	1.16	1.11
H_2O^-	0.11	0.14	0.10
F(ekv)	–0.064	–0.060	–0.010
Total	99.97	99.36	99.62
V	59	59	70
Co	15	14	17
Cr	237	261	244
Ni	78	102	63
Cu	21	24	13
Zn	68	71	66
As	9	< 1	7.9
Rb	353	358	352
Sr	312	294	337
Y	19	18	21
Zr	346	296	356
Nb	26	25	29
Mo	<1	<1	<7
Sn	14	17	<7
Pb	44	50	45
Th	n.a.	38	n.a.
U	18	18	20
La	45.0		48.37
Ce	113		101.46
Pr	12.5		14.11
Nd	56.3		57.72
Sm	15.55		12.08
Eu	1.84		1.74
Gd	8.15		6.66
Tb	0.9		<0.9
Dy	4.98		4.24
Ho	1.64		0.7
Er	3.49		1.96
Tm	0.37		<0.4
Yb	2.6		1.98
Lu	0.38		0.26
Σ REE	267		251

* from Babůrek et al. (2000)

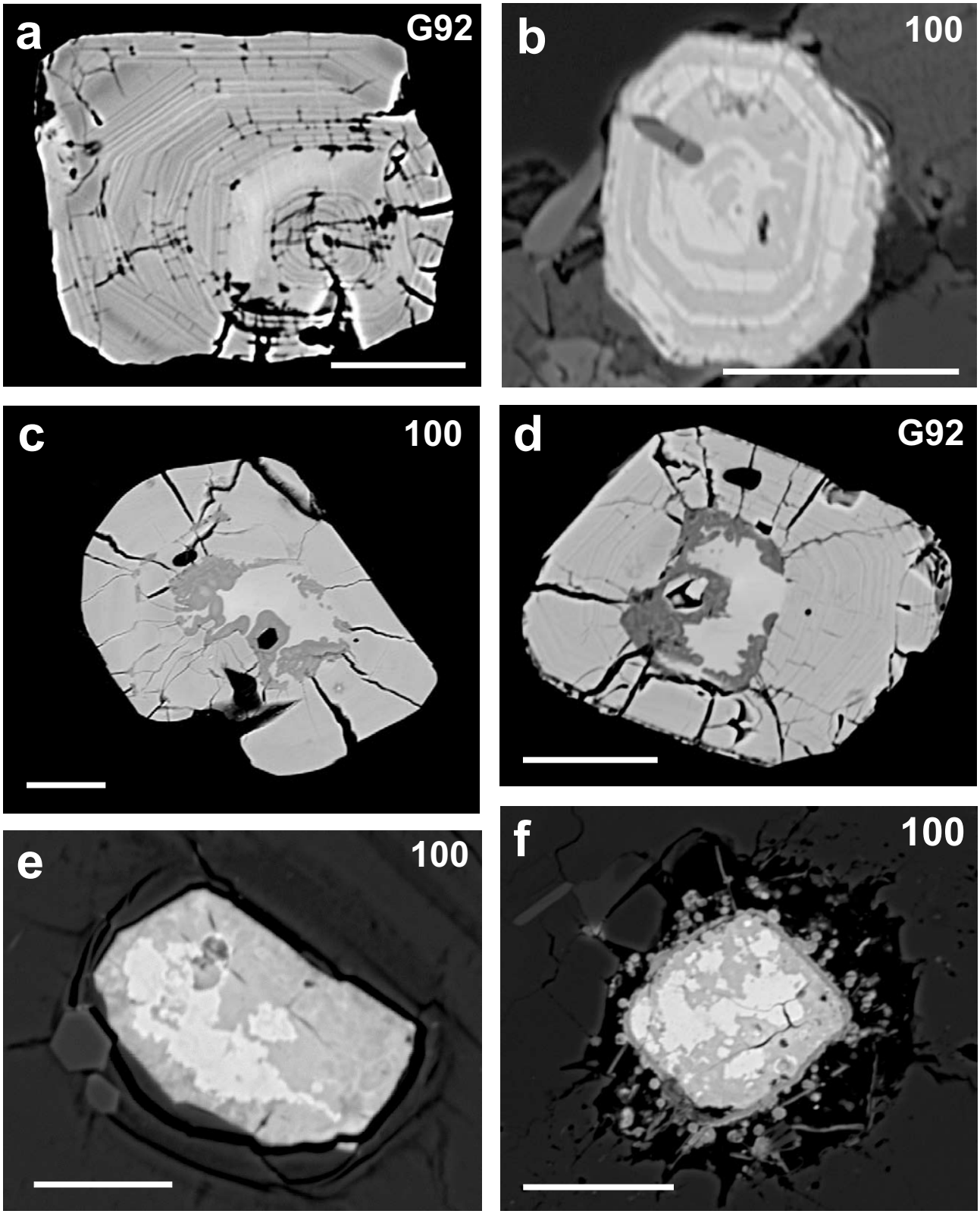

Fig. 4 The back-scattered electron (BSE) images of zircons and thorite from melasyenite porphyry (samples G92 and 100). Scale bar represents 20 μm in all photos. **a –** Primary magmatic zircon with well preserved oscillatory zoning. **b–d** Hydrothermally altered zircons: primary magmatic zircon is dark in BSE, secondary zircon is light in BSE. **e–f** Crystals of altered thorite. Photos by P. Sulovský and R. Čopjaková.

image show strong oscillatory zoning as well as obvious alteration features. ***Zircon*** is abundant as euhedral, shortly prismatic crystals, 20–100 μm in size. Most zircons show a weak igneous oscillatory zoning in the BSE images (Fig. 4a–b). The following internal features were observed in the BSE image in some large zircon grains: *central bright cores,* which are often replaced by *darker zones*. Both the zones are surrounded by thick, *weakly to strongly oscillatory zoned rims* often containing radial fractures (see Fig. 4c–d). Subhedral to anhedral crystals of ***thorite*** are equant and their size ranges between 5 and 50 μm. It is less abundant than zircon or allanite, but due to the high brightness in the BSE image it is easily identified in the thin section. Thorite is usually strongly altered and full of cracks. The altered domains are darker in the BSE image and propagate irregularly from the rims inwards (Fig. 4d–e). If the thorite is hosted by mica or feldspar, a damage zone caused by irradiation surrounds the thorite grain (Fig. 4f). Scarce **monazite** found only in the sample G92 forms small subhedral to euhedral crystals up to 20 μm, homogeneous in the BSE image.

3. Methods

The field gamma spectrometry measurements were carried out with GRM-260/B gamma spectrometer, magnetic susceptibility was measured in field using KT-5 kappameter.

Mineral microanalyses were obtained from polished and carbon-coated thin sections on the electron microprobe Cameca SX-100 (Joint Laboratory of the Masaryk University and the Czech Geological Survey) in the WDS mode. Zircon, thorite, monazite were analysed using an accelerating voltage and beam current of 15 kV and 20–40 nA, respectively, and with a beam diameter ranging from >1 to 2 μm. Variable conditions were employed to reduce the damage of hydrated phases. The following standards were used: U – metallic U, Pb – PbSe, Th – ThO_2, P – fluorapatite, Y – YAG, La – LaB_6, Ce – $CeAl_2$, Pr – PrF_3, Nd – NdF_3, Sm – SmF_3, Gd – GdF_3, Dy – $DyPO_4$, Er – YErAG, Yb – YbAG, Al – almandine, Si, Ca, Fe – andradite, Mn – rhodonite, W – scheelite, S – baryte, F – topaz, As – InAs, Nb – columbite, Ta – $CrTa_2O_6$, Ti – titanite, Zr – zircon, and Sc – $ScVO_4$, Mg – pyrope, Sr – $SrSO_4$. Raw data were reduced by the PAP correction (Pouchou and Pichoir 1985).

The mineral formulae of zircon, thorite and monazite are based on 4 oxygens, the allanite formulae were calculated on the basis of three Si atoms.

In order to estimate the degree of radiation damage in zircons, the total cumulative dose of the α-decay D_α was calculated according the equation published by Ewing et al. (2003):

$$D_\alpha = 8(C_U N_A 0{,}9928)/(M_{238}10^6)(e^{\lambda 238 t}-1)+7(C_U N_A 0{,}0072)/(M_{235}10^6)(e^{\lambda 235 t}-1)+6(C_{Th}N_A)/(M_{232}10^6)(e^{\lambda 232 t}-1),$$

where C_U, and C_{Th} are concentrations of U and Th (in ppm), respectively; N_A is the Avogadro's number. The M_{238}, M_{235}, and M_{232} are the molar weights and λ_{238}, λ_{235}, and λ_{232} are half-lives of the respective ^{238}U, ^{235}U, and ^{232}Th isotopes and the t stands for the geological age.

The D_α could be converted to a radiation dose, in units of displacements-per-atom (dpa), by equation for the zircon:

$$D_{[dpa]} = (912D_{\alpha 238}+992D_{\alpha 235}+989D_{\alpha 232})M/(6N_A),$$

where the 912, 992 and 989 is a number of generated displacements during one decay of $^{238}U\rightarrow^{206}Pb$, $^{235}U\rightarrow^{207}Pb$ a $^{232}Th\rightarrow^{208}Pb$, respectively, and M is the molar weight of zircon. The numbers of displacements were obtained from Monte-Carlo computer simulations and published by e.g. Nasdala et al. (2001). With respect to possible errors, the previous equation is simplified by Nasdala et al. (2001) to $D_{[dpa]} = (940D_\alpha M)/(6N_A)$.

4. Results

4.1. Chemical composition of the accessory minerals

Titanite, apatite, allanite, zircon, thorite and monazite are the possible carriers of radioactive elements in the melasyenite porphyry.

Titanite is enriched in REE and Nb (0.5–1.5 wt. % ΣREE, 0.13–0.95 wt. % Nb_2O_5). The content of U and Th is below detection limit of the EMPA.

Fluorapatite displays higher F (2.08–3.41 wt. %), and elevated REE contents (0.62–0.87 wt. % $REE_2O_3+Y_2O_3$). The amount of Y_2O_3 is below 0.077 wt. %. The content of U and Th is below detection limit of the EMPA.

Allanite-(Ce) does not show significant compositional variability despite strong oscillatory zoning observed in the BSE. The Ca content ranges between 0.933 and 1.175 apfu (9.43–11.57 wt. % CaO) and the sum of Y, REE varies from 0.647 to 0.777 apfu (19.96–22.47 wt. % Y, REE_2O_3) with the dominance of Ce (0.325–0.384 apfu; 11.07–9.43 wt. % Ce_2O_3). The amount of Th ranges from 0.004 to 0.026 apfu (0.20–1.22 wt. % ThO_2) and predominates over U (0.002 apfu; 0.11 wt. % UO_2). The presence of Mg (0.111–0.168 apfu; 1.04–1.19 wt. % MgO) corresponds to 11–17 % of the dissakisite molecule. The concentration of F is low (≤0.091 apfu; ≤0.31 wt. %); for details see Tab. 2. Chemical analyses of the allanite disclose its slight alteration. The analytical totals of oxides including the calculated water vary from 94 to 98 wt. %;

Table 2. Chemical composition of allanite-(Ce). The mineral formulae were calculated on the basis of 3 Si atoms

	100A	G92	G92
P_2O_5	0.09	0.00	0.08
SiO_2	31.66	32.31	32.48
TiO_2	0.39	0.64	1.70
ThO_2	0.20	0.19	1.22
UO_2	0.06	0.00	0.06
Al_2O_3	17.03	17.15	14.71
Y_2O_3	0.00	0.14	0.08
La_2O_3	6.18	5.55	5.74
Ce_2O_3	11.07	11.02	9.94
Pr_2O_3	0.87	0.82	0.86
Nd_2O_3	3.66	4.04	2.73
Sm_2O_3	0.51	0.61	0.45
Gd_2O_3	0.18	0.27	0.16
MgO	1.04	0.92	1.02
CaO	11.57	11.35	9.43
MnO	0.24	0.30	0.41
FeO	10.72	11.39	11.01
Na_2O	0.12	0.00	0.00
F	0.30	0.28	0.31
H_2O_{calc}	1.44	1.48	1.48
O=F	-0.13	-0.12	-0.13
Total	97.20	98.34	93.74
P^{5+}	0.007	0.000	0.006
Si^{4+}	3.000	3.000	3.000
Ti^{4+}	0.028	0.045	0.118
Th^{4+}	0.004	0.004	0.026
U^{4+}	0.001	0.000	0.001
Al^{3+}	1.902	1.877	1.601
Y^{3+}	0.000	0.007	0.004
La^{3+}	0.216	0.190	0.196
Ce^{3+}	0.384	0.375	0.336
Pr^{3+}	0.030	0.028	0.029
Nd^{3+}	0.124	0.134	0.090
Sm^{3+}	0.017	0.020	0.014
Gd^{3+}	0.006	0.008	0.005
Mg^{2+}	0.147	0.127	0.140
Ca^{2+}	1.175	1.129	0.933
Mn^{2+}	0.019	0.024	0.032
Fe^{2+}	0.850	0.884	0.850
Na^+	0.022	0.000	0.000
F^-	0.090	0.082	0.091
H^+	0.910	0.918	0.909
O^{2-}	12.713	12.636	12.084
Sum	7.931	7.851	7.383

negative correlation was observed between analytical totals and Th contents. Due to the alteration, the Fe^{2+}/Fe^{3+} ratios were not calculated from the formula but some approximation is indicated in Fig. 5a. The chondrite-normalized REE pattern is plotted in Fig. 5b.

Zircon shows large chemical variability; the distinct zones observed in BSE vary in chemical composition.

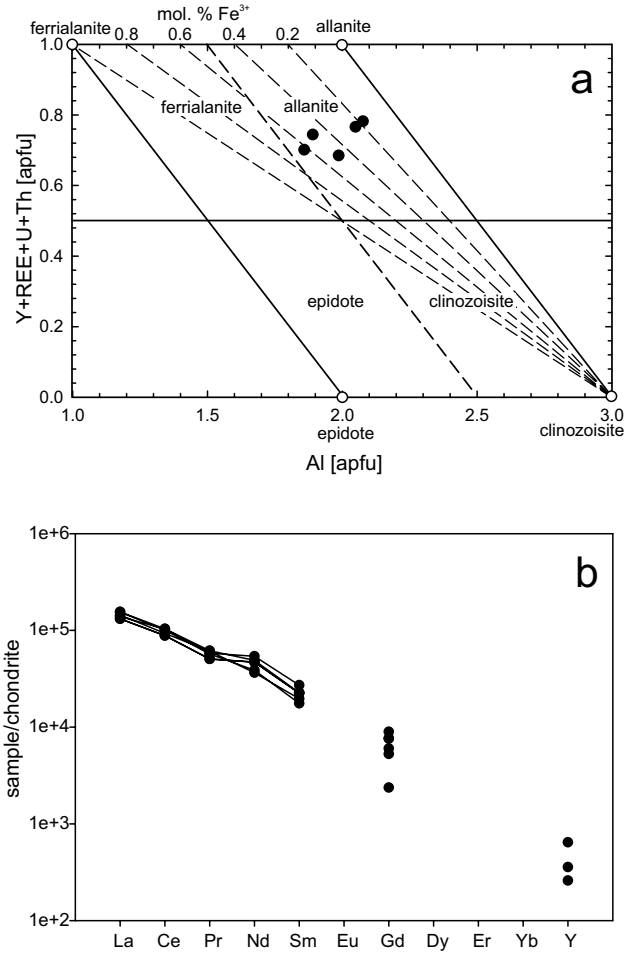

Fig. 5 Chemical composition of allanite-(Ce). **a** – The plot of Al vs. Y + REE + Ca + U + Th modified after Petrík et al. (1995). **b** – Chondrite-normalized REE pattern of allanite-(Ce); normalization data by Taylor and McLennan (1985).

The *central bright core* is enriched in U (0.005–0.010 apfu; 0.66–1.36 wt. % UO_2) and Th (0.001–0.007 apfu; 0.21–0.94 wt. % ThO_2). The sum of Y, REE (0.002–0.011 apfu; 0.15–0.73 wt. % $REE_2O_3 + Y_2O_3$) prevails over P (≤0.003 apfu; ≤0.12 wt. % P_2O_5). Hafnium content varies in a narrow range (0.010–0.012 apfu; 0.94–1.37 wt. % HfO_2). The analytical totals of oxides are high (98–99 wt. %).

The *darker zone* shows a strong deviation from the ideal formula. It is highly enriched in Ca (up to 0.189 apfu; 5.19 wt. % CaO), Fe (up to 0.020 apfu; 0.7 wt. % FeO) and Al (up to 0.017 apfu; 0.42 wt. % Al_2O_3). The contents of U and Th are elevated (0.007–0.016 apfu; 0.95–2.15 wt. % UO_2 and 0.008–0.013 apfu; 0.99–1.67 wt. % ThO_2). The sum of Y and REE does not exceed 0.024 apfu (1.81 wt. % $REE_2O_3 + Y_2O_3$), whereas in some analyses (La or Ce) > Y. The content of P is lower, up to 0.007 apfu (0.23 P_2O_5). The analytical totals of oxides are 91–95 wt. %. The thick *oscillatory-zoned rim* cor-

Table 3. Chemical composition of zircon and thorite. The mineral formulae were calculated on the basis of 4 anions

	zircon				thorite							
	G92	G92	G92	100A	G92	G92	G92	100A	100A	100A	100A	100A
SO_3	0.00	0.00	0.00	0.00	0.59	2.22	0.27	0.31	0.54	0.07	0.39	0.38
WO_3	0.00	0.00	0.00	0.00	0.15	0.14	0.05	0.09	0.11	0.08	0.15	0.11
P_2O_5	0.00	0.08	0.06	0.00	1.64	0.64	0.25	3.69	4.89	2.89	0.22	0.22
As_2O_5	0.00	0.00	0.00	0.00	0.59	1.05	0.00	0.58	0.91	0.59	0.00	0.00
SiO_2	31.77	31.75	26.04	31.55	16.42	10.98	20.77	12.29	13.92	14.44	20.79	21.07
TiO_2	0.00	0.00	0.00	0.00	0.07	0.24	0.00	0.76	0.09	0.60	0.00	0.00
ZrO_2	65.04	64.55	49.67	64.07	0.53	0.08	0.00	4.25	0.52	11.96	0.09	0.08
HfO_2	1.39	1.37	0.91	1.47	0.00	0.00	0.00	0.00	0.00	0.00	0.00	0.00
ThO_2	0.13	0.29	2.02	0.09	50.06	50.60	58.03	53.42	57.02	42.91	37.27	39.21
UO_2	0.33	0.59	2.14	0.32	5.76	2.62	11.18	1.79	9.04	7.46	27.60	24.54
Al_2O_3	0.00	0.00	0.22	0.00	0.51	1.03	0.63	1.24	0.76	1.15	1.18	1.17
Y_2O_3	0.00	0.00	0.27	0.00	2.37	0.00	0.22	0.10	0.52	0.39	0.53	0.60
La_2O_3	0.00	0.00	0.00	0.00	0.62	0.15	0.00	0.21	0.40	0.22	0.92	0.83
Ca_2O_3	0.00	0.00	0.00	0.00	3.75	1.80	0.10	0.72	1.79	1.49	2.74	2.77
Pr_2O_3	0.00	0.00	0.00	0.00	0.53	0.00	0.00	0.16	0.21	0.20	0.41	0.34
Nd_2O_3	0.00	0.06	0.00	0.08	2.88	0.00	0.27	0.36	1.10	1.03	1.74	1.78
Sm_2O_3	0.00	0.00	0.00	0.00	0.95	0.00	0.06	0.07	0.33	0.25	0.25	0.32
Gd_2O_3	0.00	0.00	0.00	0.00	0.95	0.00	0.09	0.12	0.36	0.26	0.38	0.46
Dy_2O_3	0.00	0.00	0.00	0.00	0.40	0.00	0.06	0.00	0.00	0.00	0.00	0.13
Er_2O_3	0.00	0.00	0.00	0.00	0.21	0.00	0.00	0.00	0.00	0.00	0.06	0.07
Yb_2O_3	0.07	0.10	0.08	0.08	0.17	0.00	0.00	0.00	0.06	0.07	0.00	0.00
Bi_2O_3	0.13	0.12	0.06	0.12	0.16	0.14	0.13	0.07	0.15	0.12	0.13	0.09
PbO	0.00	0.00	0.10	0.00	0.08	0.23	0.30	0.27	0.14	0.28	0.83	0.70
MgO	0.00	0.00	0.16	0.00	0.00	0.05	0.06	0.12	0.00	0.00	0.11	0.09
CaO	0.00	0.00	0.63	0.00	1.38	1.35	1.80	0.52	0.55	0.36	1.02	1.04
MnO	0.00	0.00	0.00	0.00	0.00	0.09	0.09	0.00	0.00	0.00	0.00	0.00
FeO	0.32	0.14	0.47	0.29	3.69	3.98	0.54	6.12	4.48	7.36	0.37	0.32
F	0.00	0.00	0.00	0.00	0.24	0.16	0.30	0.00	0.23	0.07	0.52	0.59
O=F	0.00	0.00	0.00	0.00	-0.10	-0.07	-0.13	0.00	-0.10	-0.03	-0.22	-0.25
Total	99.18	99.05	82.83	98.07	94.60	77.48	95.07	87.26	98.02	94.22	97.48	96.66
S^{6+}	0.000	0.000	0.000	0.000	0.023	0.106	0.010	0.013	0.020	0.003	0.014	0.014
W^{6+}	0.000	0.000	0.000	0.000	0.002	0.002	0.001	0.001	0.001	0.001	0.002	0.001
P^{5+}	0.000	0.002	0.002	0.000	0.071	0.035	0.011	0.170	0.207	0.119	0.009	0.009
As^{5+}	0.000	0.000	0.000	0.000	0.016	0.035	0.000	0.017	0.024	0.015	0.000	0.000
Si^{4+}	0.990	0.992	0.992	0.994	0.843	0.701	1.054	0.670	0.695	0.701	1.026	1.038
Ti^{4+}	0.000	0.000	0.000	0.000	0.003	0.012	0.000	0.031	0.003	0.022	0.000	0.000
Zr^{4+}	0.989	0.983	0.922	0.984	0.013	0.002	0.000	0.113	0.013	0.283	0.002	0.002
Hf^{4+}	0.012	0.012	0.010	0.013	0.000	0.000	0.000	0.000	0.000	0.000	0.000	0.000
Th^{4+}	0.001	0.002	0.018	0.001	0.585	0.736	0.670	0.662	0.648	0.474	0.419	0.439
U^{4+}	0.002	0.004	0.018	0.002	0.066	0.037	0.126	0.022	0.100	0.081	0.303	0.269
Al^{3+}	0.000	0.000	0.010	0.000	0.031	0.078	0.038	0.080	0.045	0.066	0.069	0.068
Y^{3+}	0.000	0.000	0.005	0.000	0.065	0.000	0.006	0.003	0.014	0.010	0.014	0.016
La^{3+}	0.000	0.000	0.000	0.000	0.012	0.004	0.000	0.004	0.007	0.004	0.017	0.015
Ce^{3+}	0.000	0.000	0.000	0.000	0.071	0.042	0.002	0.014	0.033	0.026	0.049	0.050
Pr^{3+}	0.000	0.000	0.000	0.000	0.010	0.000	0.000	0.003	0.004	0.004	0.007	0.006
Nd^{3+}	0.000	0.001	0.000	0.001	0.053	0.000	0.005	0.007	0.020	0.018	0.031	0.031
Sm^{3+}	0.000	0.000	0.000	0.000	0.017	0.000	0.001	0.001	0.006	0.004	0.004	0.005
Gd^{3+}	0.000	0.000	0.000	0.000	0.016	0.000	0.002	0.002	0.006	0.004	0.006	0.008
Dy^{3+}	0.000	0.000	0.000	0.000	0.007	0.000	0.001	0.000	0.000	0.000	0.000	0.002
Er^{3+}	0.000	0.000	0.000	0.000	0.003	0.000	0.000	0.000	0.000	0.000	0.001	0.001
Yb^{3+}	0.001	0.001	0.001	0.001	0.003	0.000	0.000	0.000	0.001	0.001	0.000	0.000
Bi^{3+}	0.001	0.001	0.001	0.001	0.002	0.002	0.002	0.001	0.002	0.002	0.002	0.001
Pb^{2+}	0.000	0.000	0.001	0.000	0.001	0.004	0.004	0.004	0.002	0.004	0.011	0.009
Mg^{2+}	0.000	0.000	0.009	0.000	0.000	0.005	0.005	0.010	0.000	0.000	0.008	0.007
Ca^{2+}	0.000	0.000	0.026	0.000	0.076	0.092	0.098	0.030	0.029	0.019	0.054	0.055
Mn^{2+}	0.000	0.000	0.000	0.000	0.000	0.005	0.004	0.000	0.000	0.000	0.000	0.000
Fe^{2+}	0.008	0.004	0.015	0.008	0.158	0.213	0.023	0.279	0.187	0.299	0.015	0.013
F^-	0.000	0.000	0.000	0.000	0.039	0.032	0.048	0.000	0.036	0.011	0.081	0.092
O^{2-}	4.000	4.000	4.000	4.000	3.961	3.968	3.952	4.000	3.964	3.989	3.919	3.908
Sum	2.005	2.002	2.029	2.004	2.146	2.111	2.060	2.137	2.066	2.157	2.063	2.060

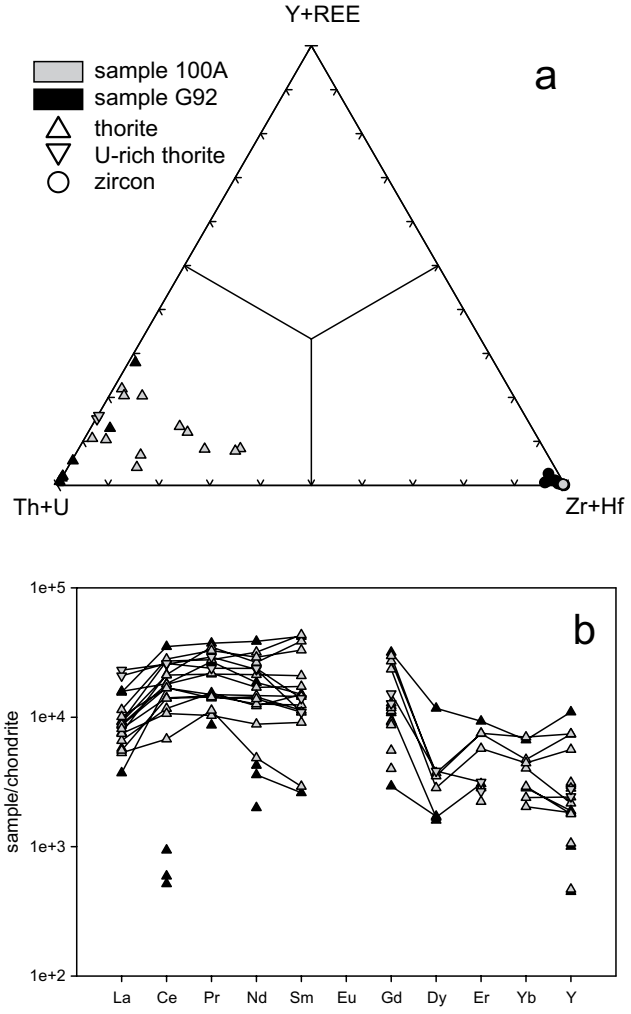

Fig. 6a – Chemical variability of thorite and zircon in the diagram of the system (Th,U)SiO_4 – (Zr,Hf)SiO_4 – (Y,REE)PO_4. **b –** Chondrite-normalized REE pattern of thorite; normalization data by Taylor and McLennan (1985).

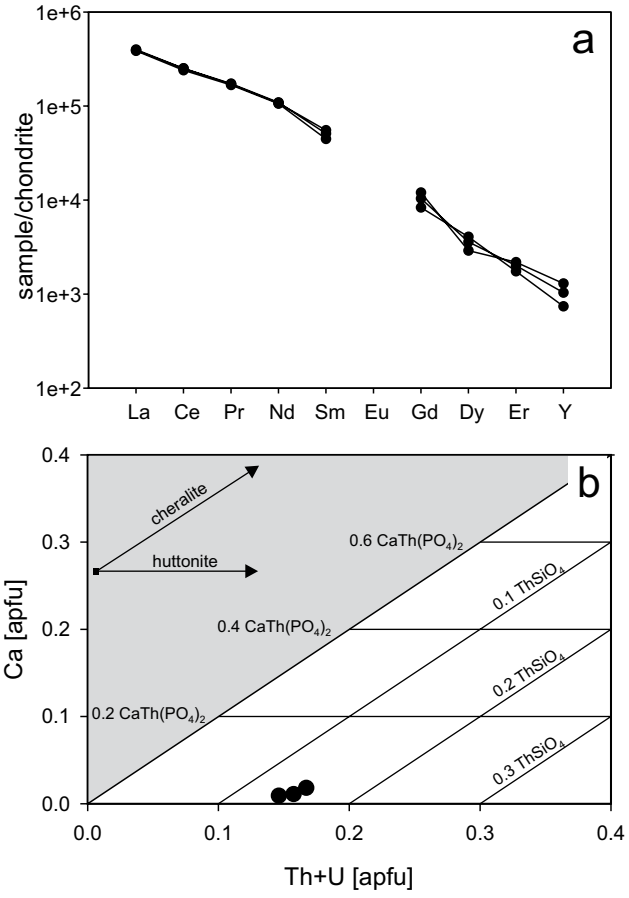

Fig. 7a – Chondrite-normalized REE pattern of monazite-(Ce); normalization data by Taylor and McLennan (1985). **b –** Monazite compositional end-members expressed in Th+U vs. Ca plot.

responds to the nearly ideal stoichiometric zircon with 0.010–0.013 apfu Hf (1.13–1.47 wt. % HfO_2). The U and Th contents are lower than in previously described parts, attaining up to 0.003 apfu U (0.42 wt. % UO_2) and up to 0.001 apfu Th (0.13 wt. % ThO_2). The sum of Y and REE does not exceed 0.002 apfu (0.19 Y,REE_2O_3). The Zr/(Hf + Zr) ratios of the *central bright core* and *darker zone* are the same in individual crystals but do slightly vary for the grains studied (0.010–0.011). Representative chemical analyses are in Tab. 3. The Zr/(Hf + Zr) ratios in the *oscillatory zoned rim* are always higher than in the inner parts and vary from 0.012 to 0.016.

Thorite appears patchily but strongly altered in the BSE image (Fig. 4e–f). The total of oxides in pristine, little altered areas is higher (95–98 wt. %) than in the altered zones where it drops down to 77 wt. % (Tab. 3). The U content varies in range 1.79–27.60 wt. % UO_2 (0.022–0.303 apfu). The Si content is variable (0.609–1.054 apfu; 10.30–21.07 wt. % SiO_2), whereas the lowest amount is in the most hydrated areas. The Zr contents vary significantly (0.000–0.270; 0.00–10.92 wt. % ZrO_2) as do P (0.005–0.249; 0.22–6.39 wt. % P_2O_5) and Y,REE (0.016–0.257; 0.73–12.81 wt. % REE_2O_3) (Fig. 6a). The Y,REE and Si are strongly depleted in more hydrated parts. Among the Y,REE, the most abundant are Ce, Nd and Y. The chondrite-normalized REE pattern is plotted on Fig. 6b. Studied thorites show unusually high amount of Fe (0.013–0.187 apfu; 0.32–4.48 wt. % FeO) and up to 0.546 apfu (12.87 wt. % FeO) in the highly hydrated areas. The Ca content does not exceed 0.09 apfu (1.36 wt. % CaO). Elevated amounts of PbO < 0.83, As_2O_5 < 1.76, Al_2O_3 < 1.28, SO_3 < 2.22, and TiO_2 < 0.69 (all in wt. %) were observed specially in the most hydrated parts.

Monazite-(Ce) strongly concentrates LREE, with cerium as the most abundant rare earth element. The chondrite-normalized REE pattern is presented on Fig. 7a. Monazite is enriched in radioactive elements.

Thorium (0.126–0.150 apfu; 13.57–15.85 wt. % ThO_2) prevails over uranium (0.014–0.017 apfu; 1.51–1.91 wt. % UO_2). Silica ranges from 0.146 to 0.159 apfu (3.56–3.83 wt. % SiO_2), the Ca is low, up to 0.018 apfu (0.41 wt. % CaO); for the details see Tab. 4. Positive correlation of the U + Th and Si close to 1:1 shows evidence for huttonite substitution $(Y,REE)PTh_{-1}Si_{-1}$, up to 16 % of the huttonite molecule. The cheralite substitution $(Y,REE)_2Ca_{-1}(U,Th)_{-1}$ is only of minor importance (up to 4 % of cheralite molecule), see Fig. 7b.

Table 4. Chemical composition of the monazite-(Ce) from the sample G92. The mineral formulae were calculated on the basis of 4 anions

P_2O_5	24.14	25.15	P^{5+}	0.850	0.871
SiO_2	3.83	3.56	Si^{4+}	0.159	0.146
ThO_2	15.85	13.57	Th^{4+}	0.150	0.126
UO_2	1.51	1.91	U^{4+}	0.014	0.017
Y_2O_3	0.16	0.28	Y^{3+}	0.004	0.006
La_2O_3	15.40	15.62	La^{3+}	0.236	0.236
Ca_2O_3	25.64	26.76	Ce^{3+}	0.391	0.401
Pr_2O_3	2.37	2.42	Pr^{3+}	0.036	0.036
Nd_2O_3	7.90	8.03	Nd^{3+}	0.117	0.117
Sm_2O_3	1.01	1.25	Sm^{3+}	0.014	0.018
Gd_2O_3	0.25	0.36	Gd^{3+}	0.003	0.005
Dy_2O_3	0.14	0.10	Dy^{3+}	0.002	0.001
Er_2O_3	0.04	0.05	Er^{3+}	0.001	0.001
CaO	0.41	0.21	Ca^{2+}	0.018	0.009
PbO	0.28	0.25	Pb^{2+}	0.003	0.003
Total	98.93	99.52	Sum	1.999	1.993

4.2. Zircon radiation damage

The calculated radiation damage for zircon expressed in displacements per atom ($D_{[dpa]}$) varies from 0.0548 to 0.9942. The lowest values were recorded in the grains with the lowest U and Th concentrations from the homogeneous, oscillatory-zoned rim, compared to the highest values from the central part and the intermediate darker zone.

5. Discussion

5.1. Chemical composition of zircon and thorite

Entry of Y and REE into the zircon and thorite structure is generally ascribed to the xenotime substitution $(Y,REE)PZr_{-1}Si_{-1}$, $(Y,REE)PTh_{-1}Si_{-1}$. This substitution plays a negligible role in the studied zircon and thorite, though. The number of the Y,REE atoms is not compensated by sufficient amounts of P or other pentavalent ions (Fig. 8).

Hoskin (2000) described incorporation of the Y,REE into the interstitial positions of zircon by the following substitutions: $^{int}(Mg,Fe)^{2+}(Y,REE)^{3+}{}_3P^{5+}Zr^{4+}{}_{-3}Si^{4+}{}_{-1}$ and $^{int}(Al,Fe)^{3+}(Y,REE)^{3+}{}_4P^{5+}Zr^{4+}{}_{-4}Si^{4+}{}_{-1}$. These substitutions are not important in the studied zircons, either. The concentrations of Th are much lower than those of U, which is in accord with the general preference of the zircon structure for smaller U (Hoskin and Schaltegger 2003).

The chondrite-normalized REE pattern of thorite (Fig. 6b) shows enrichment in LREE over HREE, and the molar content of Y is mostly lower than Ce. It differs significantly from the REE patterns published in literature (e.g. Förster 2006), which are typically enriched in HREE.

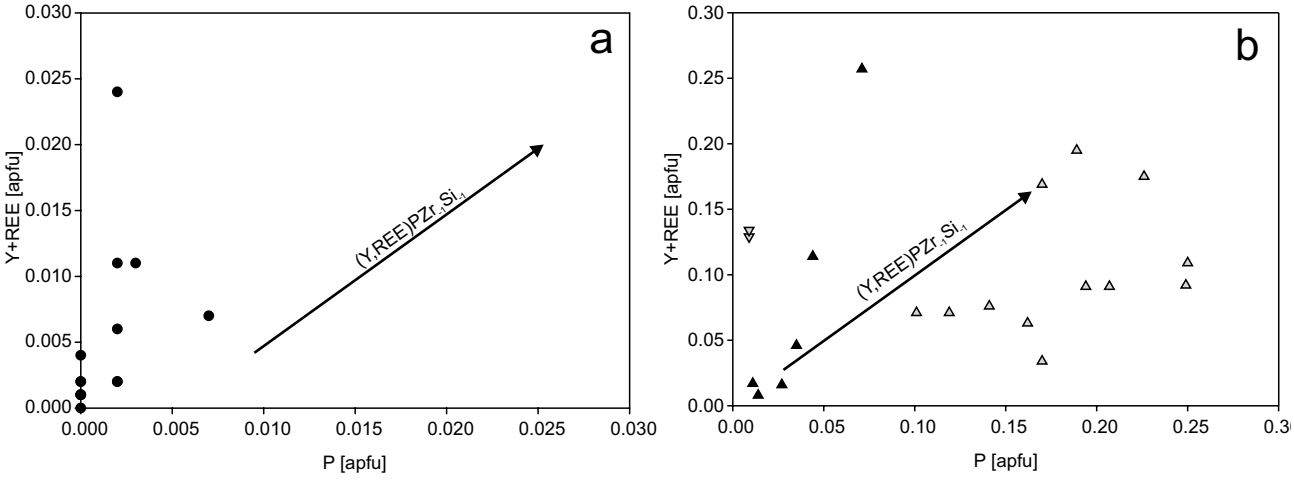

Fig. 8 Absence of the xenotime substitution in zircon (a) and thorite (b).

Förster et al. (2000) argued that the monoclinic $ThSiO_4$ (huttonite – isostructural with monazite) prefers LREE while the tetragonal $ThSiO_4$ (thorite – isostructural with zircon) prefers HREE (Bea 1996). According to experimental results published by Grover and Tyagi (2005), some 0.1 apfu Ce stabilizes the tetragonal modification of $ThSiO_4$. Huttonite is more resistant to metamictization than thorite is (Meldrum et al. 1999). With respect to the low analytical totals (77–97 wt. % oxides) and the Zr contents (≤ 0.27 apfu) we classify the studied $ThSiO_4$ phases as thorite.

The highest reported U contents in thorite from granitic rocks were from Ririwai granite, Nigeria (28.9 wt. % of UO_2; Pointer et al. 1988) and the Kirchberg Pluton, the Erzgebirge (23.3 wt. % of UO_2; Förster 2006). The values from sample 100 (≤ 27.6 wt. % of UO_2) belong to the highest contents reported up to date.

5.1.1. Miscibility in the system $(Zr,Hf)SiO_4$–$(Th,U)SiO_4$–$(Y,REE)PO_4$

Förster (2006) described a complete solid solution between zircon, thorite + coffinite, and xenotime from the Erzgebirge granites. Miscibility in studied zircons is limited, up to 3.7 mol. % of thorite + coffinite and up to 2.6 mol. % of xenotime. Despite the uncertainties regarding the Y, REE entry into the zircon structure described above, the xenotime component was calculated as molar occupancy of Y and REE in the appropriate structural site. On the other hand, the miscibility between thorite and zircon (with hafnon) is higher, up to 31.8 mol. % as well as $(Y,REE)PO_4$ component up to 27.9 mol. %. Thorite from sample 100 is more enriched in zircon molecule (with contemporaneous enrichment of $(Y,REE)PO_4$ component from 4.0 to 22.0 mol. %) than thorite from the sample G92. Its variability in chemical composition is limited to the solid solution of thorite – $(Y,REE)PO_4$ only (from nearly pure thorite to 27.9 mol. % $(Y,REE)PO_4$, and up to 3.9 mol. % zircon). For details see Fig. 6a.

5.2. Radiation-induced structural damage and anomalous composition

Geisler et al. (2003b) carried out a hydrothermal experiment on zircon samples with different degrees of radiation damage. They found jumps in the alteration rate with regard to the increasing radiation damage of zircon. The first dramatic increase (the first percolation point) sets in when the amorphous domains form interconnected clusters in the structure. Reaching this point in natural samples can be accompanied by a dramatic increase in Ca, Al, Fe and other "non-formula" elements (Geisler et al. 2003c) as well as a decrease in Si accompanied by a strong hydratation. The amounts of Ca, Al and Fe are low up to 0.4 $D_{[dpa]}$, then their contents increase dramatically. The first percolation point was reached at about 0.4 $D_{[dpa]}$ (Fig. 9). Published $D_{[dpa]}$ values of the first percolation point in zircon vary from 0.05 (Hoskin 2000, 2005), through 0.07 (Davis and Krogh 2000), 0.11 (Škoda et al. 2009), 0.76 (Utsunomiya et al. 2007) to 0.95 (Geisler et al. 2003a). Values of the first percolation point could be strongly dependent on thermal

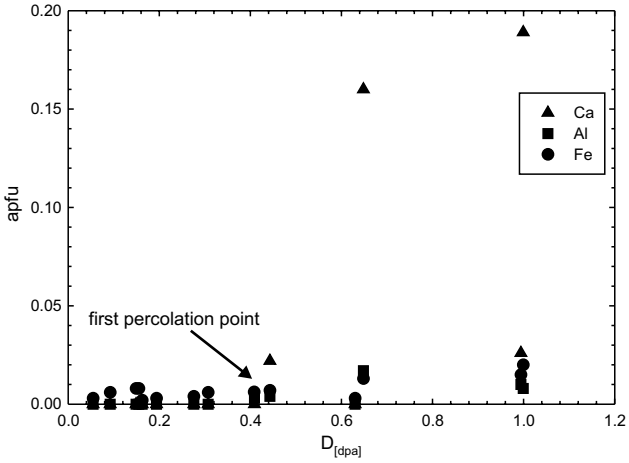

Fig. 9 Dependence of "non-formula" elements contents on the radiation damage degree.

history of zircon (Geisler 2003a) as well as amounts and mineralization of hydrothermal fluids. This is because the increased temperature promotes thermal annealing of the structure. Temperatures about 100–200 °C decrease the amorphization rate (Ewing et al. 2003). The entry of Ca, Fe, Al, S, As, Ti and other "non-formula" elements into thorite and the removal of the original components by post-magmatic, low-temperature fluids (in a similar way as in zircon) is very probable. The interaction between the metamict mineral and hydrothermal fluid results in changes in chemical composition, whereby the primary substitution mechanisms are obscured. Metamictization and hydration lead to the volume expansion and consequent formation of the cracks. These fractures enhanced fluid flux and related interaction processes.

6. Conclusions

Zircon, thorite and allanite-(Ce) are the most important carriers of U and Th in the studied ultrapotassic melasyenite porphyries from the Šumava Mts. Among the accessory minerals with the low concentrations of U and Th, titanite and apatite are the most abundant. Although some zircon grains preserve well magmatic zoning, most show effects of secondary alteration. The thorite represents limited solid solution of thorite–zircon and thorite–$(Y,REE)PO_4$. Its chemical composition is strongly affected by late, post-magmatic hydrothermal activity.

The scarcity of monazite in the melasyenite porphyry reflects the whole-rock composition and corresponds to the situation in larger durbachite massifs (Sulovský 2001). The melasyenite dykes can cause locally intense but very small-scale radiometric anomalies, which are mostly undetectable by previous airborne gamma spectrometric measurements.

Acknowledgements The manuscript was substantially improved by the detailed reviews by P. Uher and V. Goliáš, as well as careful editing by M. Štemprok and V. Janoušek. This work was supported by the GAAV KJB30163080 and GAČR 205/07/1159 research projects.

Electronic supplementary material. The GPS coordinates of the studied samples are available online at the Journal web site *(http://dx.doi.org/10.3190/jgeosci.053)*.

References

Babůrek J, Fürich V, Goliáš V, Hanžl P, Kadlecová R, Lhotský P, Nekovařík Č, Nývlt D, Osterrothová K, Pertoldová J, Strnad L, Šebesta J, Vlčková L (2000) Explanatory notes and basic geological map of the Czech Republic, scale 1:25 000, sheet 22-332 Kašperské Hory. Unpublished manuscript, Czech Geological Survey. Prague (in Czech)

Bea F (1996) Residence of REE, Y, Th and U in granites and crustal protoliths; implications for the chemistry of crustal melts. J Petrol 37: 521–552

Davis DW, Krogh TE (2000) Preferential dissolution of ^{234}U and radiogenic Pb from a-recoil-damaged lattice sites in zircon: implications for thermal histories and Pb isotopic fractionation in the near surface environment. Chem Geol 172: 41–58

Ewing RC, Meldrum A, Wang LM, Weber, WJ, Corrales LR (2003) Radiation effects in zircon. In: Hanchar JM, Hoskin PWO (eds) Zircon. Reviews in Mineralogy and Geochemistry 53: pp 388–425

Förster HJ (2006) Composition and origin of intermediate solid solutions in the system thorite–xenotime–zircon–coffinite. Lithos 88: 35–55

Förster HJ, Harlov DE, Milke R (2000) Composition and Th–U–total Pb ages of huttonite and thorite from Gillespie's Beach, South Island, New Zealand. Canad Mineral 38: 675–684

Geisler T, Pidgeon RT, Kurtz R, van Bronswijk W, Schleicher H (2003a) Experimental hydrothermal alteration of partially metamict zircon. Amer Miner 88: 1496–1513

Geisler T, Trachenko K, Ríos S, Dove MT, Salje EKH (2003b) Impact of self-irradiation damage on the aqueous durability of zircon ($ZrSiO_4$): implications for its suitability as nuclear waste form. Jour of Physics: Condensed Matter 15: 597–605

Geisler T, Rashwan AA, Rahn MKW, Poller U, Zwingmann H, Pidgeon RT, Schleicher H, Tomaschek F (2003c) Low-temperature hydrothermal alteration of natural metamict zircons from the Eastern Desert, Egypt. Mineral Mag 67: 485–508

Grover V, Tyagi AK (2005) Preparation and bulk thermal expansion studies in $M_{1-x}Ce_xSiO_4$ (M = Th, Zr) system, and stabilization of tetragonal $ThSiO_4$. Jour of Alloys and Compounds 390: 112–114

Holub FV (1997) Ultrapotassic rocks of the durbachite series in the Bohemian Massif: petrology, geochemistry and petrogenetic interpretation. Sbor Geol Věd ložisk Geol Mineral 31: 2–24

Holub FV (2009) Ultrapotassic melasyenite and melagranite porphyries in the Central Bohemian Plutonic Complex and in the Moldanubian of Šumava. In: Kohút M, Šimon L (eds) Spoločný kongres Slovenskej a Českej geologickej spoločnosti, Zborník abstraktov a exkurzný sprievodca. Štátny geologický ústav Dionýza Štúra, Bratislava, pp 76–77 (in Czech)

Hoskin PWO (2000) Patterns of chaos: fractal statistics and the oscillatory chemistry of zircon. Geochim Cosmochim Acta 64: 1905–1923

Hoskin PWO (2005) Trace-element composition of hydrothermal zircon and the alteration of Hadean zircon from the Jack Hills, Australia. Geochim Cosmochim Acta 69: 637–648

Hoskin PWO, Schaltegger U (2003) The composition of zircon and igneous and metamorphic petrogenesis. In Hanchar J, Hoskin PWO (eds) Zircon. Mineralogical Society of America and Geochemical Society Reviews in Mineralogy and Geochemistry 53: pp 27–62

Janoušek V, Holub F (2007) The causal link between HP-HT metamorphism and ultrapotassic magmatism in collisional orogens: case study from the Moldanubian Zone of the Bohemian Massif. Proc Geol Assoc 118: 75–86

Meldrum A, Boatner LA, Zinkle SJ, Wang Shi-Xin, Wang Lu-Min, Ewing RC (1999) Effects of dose rate and temperature on the crystalline-to-metamict transformation in the ABO_4 orthosilicates. Canad Mineral 37: 207–221

Nasdala L, Wenzel M, Vavra G, Irmer G, Wenzel T, Kober B (2001) Metamictization of natural zircon: accumulation versus thermal annealing of radioactivity-induced damage. Contrib Mineral Petrol 141: 125–144

Petrík I, Broska I, Lipka J, Siman P (1995) Granitoid allanite-(Ce): substitution relations, redox conditions and REE distributions (on an example of I-type granitoids, Western Carpathians, Slovakia). Geol Carpath 46: 79–94

Pointer CM, Ashworth JR, Ixer RA (1988) The zircon–thorite mineral group in metasomatized granite, Ririwai, Nigeria 1. Geochemistry and metastable solid solution of thorite and coffinite. Mineral Petrol 38: 245–262

Pouchou JL, Pichoir F (1985) 'PAP' (φ-ρ-Z) correction procedure for improved quantitative microanalysis. Microbeam Anal. In: Armstrong JT (ed) San Francisco Press, pp 104–106

Sulovský P (2001) Accessory minerals of the Třebíč durbachite massif (SW Moravia). Miner Slov 33: 467–472

Škoda R, Klementová M, Čopjaková R (2009) Study of zircon from alkali syenite near Naloučany, Strážek Moldanubicum, Czech Republic. Acta Mus Moraviae Sci Nat 94: 47–59

Taylor SR, McLennan SM (1985) The Continental Crust: its Composition and Evolution. Oxford, Blackwell, pp 1–312

Utsunomiya S, Valley JW, Cavosie AJ, Wilde SA, Ewin RC (2007) Radiation damage and alteration of zircon from a 3.3 Ga porphyritic granite from the Jack Hills, Western Australia. Chem Geol 236: 92–111

Žáček V, Sulovský P (2005) The dyke swarm of evolved tourmaline-bearing aplitic leucogranite and its link to the Vydra Pluton (Moldanubian Batholith), Šumava Mts., Czech Republic. J Czech Geol Soc 50: 107–118

Žáček V, Břízová E, Lhotský P, Krupička J, Lysenko V, Mrnková J, Nováková D, Skácelová D, Šebesta J, Šrámek J, Verner K, Žák J (2005) Explanatory notes and basic geological map of the Czech Republic, scale 1 : 25 000, sheet 22-334 Kvilda. Unpublished manuscript, Czech Geological Survey, Prague (in Czech)